Materials Letters 289 (2021) 129398

Contents lists available at ScienceDirect

Materials Letters

journal homepage: www.elsevier.com/locate/mlblue

Charged-particle induced radioluminescence in nanoclusters of $CsPbBr_3$ perovskite quantum dots

Mátyás Hunyadi [a,*], Csaba Buga [a,b], Lóránt Csige [a], Attila Csík [a]

[a] Institute for Nuclear Research (ATOMKI), Debrecen H-4026, Hungary
[b] Doctoral School of Physics, University of Debrecen, Debrecen H-4032, Hungary

ARTICLE INFO

Article history:
Received 30 August 2020
Received in revised form 7 January 2021
Accepted 18 January 2021
Available online 27 January 2021

Keywords:
Perovskite
Quantum dots
Radioluminescence
α-Particles
Particle-detection
Pulse digitization

ABSTRACT

Charged-particle induced radioluminescence (RL) of $CsPbBr_3$ (CPB) perovskite quantum dots (QD) in their clustered state was investigated using α-particles from a radiation source. The RL response was analyzed with photomultiplier tubes (PMT) combined with the pulse-digitization technique, which enabled the evaluation of time-resolved waveforms for individual α-radiation events. The rising and decay transition times of electric pulses were found very close to the instrumental limitation, while orders of magnitude shorter than typically measured in conventional inorganic scintillators. Based on the statistical analysis of timing characteristics, our study assessed the potentials of employing perovskite nanomaterials in precise timing applications as demonstrated in a comparative measurement with a CsI(Tl) scintillator. The distribution of pulse charge was converted to luminescence intensities, which were fitted with Monte Carlo simulations giving an estimate of 2.95 photon/keV for the RL yield and 29.2% for detection efficiency (DE), referring to our mean cluster thickness of 5 QD layers.

1. Introduction

The recognition of the outstanding optical activity of perovskite quantum dots (QD) [1,2] led to intense research and quest for novel light-emitting applications [3,4] in parallel with the development of their macrocrystalline form as light-harvesting [5–7] and sensor material [8]. Especially, lead-halide compositions exhibit high photoabsorption, robust and tunable luminescence originating from unusually long charge-carrier lifetimes, defect tolerance of the band structure, and easy variability of chemical composition [9–11]. Since perovskites are typically synthesized of heavy elements, they effectively absorb energetic photons as well, which proposes their development for X-ray screens in medical and inspection imaging [12]. The bright luminescence and the exceptionally fast optical response free of afterglow effects are anticipated to achieve improved detection limits, signal-to-noise ratio and image contrast with respect to present techniques [13,14].

Inspired by the success of perovskite-based scintillators and time-resolved photoluminescence (PL) studies [15], the question of their potential radiation-sensing capabilities also emerged. Recent studies have demonstrated the spectroscopic detection of α-particles by direct-conversion in bulk $CsPbBr_3$ crystals, which were claimed competitive or even superior to traditional semiconductor-based detectors [16,17].

To our best knowledge, charged-particle induced RL in perovskite QDs has not been measured, the only approach tested them as sensitizing material in liquid scintillators [18]. The advantage of perovskite QDs in particle detection is the nanosecond-range transition times of luminescence pulses in contrast to the calorimetric detection mode in bulk perovskite crystals [16,17], however, spectroscopic information is lost, since energy deposition of traversing particles on the scale of QDs is a non-monotonous function of particle energy. A prosperous solution may be the combination of perovskite QDs as nanoscaled timing sensors with charge-integrating detectors as we demonstrated by testing CsI(Tl) scintillators covered with CPB nanocrystals.

In this study, we aimed at assessing the potentials of QD-based charged-particle detection by estimating transition-time parameters of individual α-radiation events, RL yield in terms of energy loss of α-particles and detection efficiency (DE) of CPB clusters in the present experimental arrangement.

2. Materials and methods

Caesium carbonate (Cs_2CO_3, 99.9%), lead(II) bromide ($PbBr_2$, 99%), oleylamine (OAM, technical grade 90%), oleic acid (OAC, technical grade 90%), 1-octadecene (ODE, technical grade 90%) and

* Corresponding author.
E-mail address: hunyadi.matyas@atomki.hu (M. Hunyadi).

https://doi.org/10.1016/j.matlet.2021.129398
0167-577X/

toluene (technical grade 99.9%) were used without purification. The CPB nanocrystals were synthesized using the hot-injection method reported previously with minor modifications [13].

First, Cs-oleate precursor was prepared by dissolving 400 mg Cs_2CO_3 in 15 mL ODE and 1.25 mL OAC at 100 °C. Second, 132 mg $PbBr_2$ was dissolved in the mixture of 1 mL OAC, 1 mL OAM and 10 mL ODE at 160 °C. Green luminescent nanocrystals appeared quickly after the injection of 1 mL Cs-oleate into the mixture at 160 °C. The crude suspension was centrifuged at 6000 rpm for 30 min. The sediment was dissolved in toluene and pressed through a PTFE filter with a pore size of 200 nm. Targets for the irradiation were prepared by drop-casting on soda-lime glass plates.

Two photomultiplier tubes (PMT) of Photonis XP2262 model were optically coupled to the target through a glass prism to detect RL photons in time-coincidence mode. The specified photoconversion efficiency and electron gain of PMTs were 9.5% (552 nm) and $8{\cdot}10^7$ (HV = −2000 V) respectively. The output signals were measured with digital pulse-shape analyzers CAEN V1730 (500 MS/s, 14 bit/2 V) and DT5761 (4 GS/s, 10 bit/1 V). The α-source was a radioisotopic mixture of Am-241, Pu-239, and Cm-244 emitting 5157, 5486, and 5804 keV particles, respectively, with a total activity of 2.03 kBq.

3. Results and discussion

The morphology and composition of CPB nanocrystals were characterized by ThermoFisher SCIOS 2 electron microscope in conventional scanning (SEM) and scanning transmission (STEM) imaging modes (Fig. 1a), and X-ray diffraction. The size distribution of CPB QDs peaked at 10 nm with acceptable monodispersity (Fig. 1c). QDs predominantly formed 2D clusters in dilute suspensions, which had the natural tendency to coalesce forming 3D assemblies controlled with the concentration of drop-casted suspension (Fig. 1b). The thickness of the clusters was measured by a cross-cutting technique using focused Ga^+-ion beam (FIB-SEM), which gave 66 ± 13 nm corresponding to 5 ± 1 QD-layers (Fig. 1d). The surface coverage φ of CPB clusters on the glass substrate was determined with a cathodoluminescence detector in low-vacuum SEM (LV-SEM, JEOL IT500HR) estimating a range of φ = 15 ± 5%.

The RL response of CPB clusters to exposure of α-particles was first characterized by pulse waveforms scanned with a sampling precision of 250 ps (Fig. 2a). In comparison with control measurements of natural and irradiation-related backgrounds, the pulse shape did not carry the relevant information for the event-level identification of the signal source, justifying the necessity of designing a coincidence setup with two PMTs capable of determining the spatial origin of pulses. Selecting events with the condition of time-correlation, we obtained transition times for the CPB-mediated RL exhibiting slightly upshifted and overlapping distributions with respect to those of the background events, which are close to the instrumental limits of the PMTs (Fig. 2b, c). The decay time distribution has a rather broad structure, nevertheless, it was found consistent with lifetimes reported for CPB QDs at room temperature [19].

A general prerequisite in experiments requiring fast timing signals of particles is the use of scintillators. To demonstrate the timing performance of perovskite QDs, we tested a 3 mm thick CsI(Tl) scintillator with CPB suspension deposited on its surface (Fig. 2d, e). The rising slope of CsI(Tl)-pulses has been considered fast enough in most experimental situations, however, its fluctuating fine structure may be a limiting factor when subnanosecond precision is needed. The protruding peak of CPB pulses overtakes the rising edge of CsI(Tl)-pulse improving the timing accuracy by nearly an order of magnitude in threshold-crossing triggering.

The second objective of our study was to estimate the RL yield $y = \Delta Y/\Delta E_\alpha$ of CPB clusters expressed in terms of the energy loss ΔE_α of α-particles, and the DE of the setup defined by the ratio of detected coincidence and alpha incidence rates. The principal observable is the pulse charge obtained by integrating the pulse waveform divided by the 50 Ω impedance of digitizer electronics. Correlated events show a distinct motif well separated from the background and random coincidence events (Fig. 3a), which was projected on one axis (Fig. 3b). This distribution was fitted with Monte Carlo simulations coded in GEANT4, and the RL yield was the free parameter to be determined. The simulated distributions involved convolution with electron-gain variance and threshold correction. The implemented geometry and typical RL rays are illustrated in Fig. 3c. The best fit was found at y = 2.95 photon/keV with a deviation estimated over a realistic range of target coverage φ (Fig. 3b, d). Taking into account a mean energy loss 1.5–2.0 keV in single QDs depending on the particle-stopping model applied [20], we obtain 4.5–6 photon/QD. This finding may propose the picture of competing decay channels of multiexcitonic states undergoing ultrafast radiative recombination and thermal relaxation with energy transfer to adjacent QDs by Förster coupling, eventually populating a multitude of luminescent monoexcitonic states [21,22].

The DE was derived by its calculated proportionality to the RL yield parameter referring to clusters of 5 QD-layers (Fig. 3e). The calculation was based on the simulation statistics assuming that

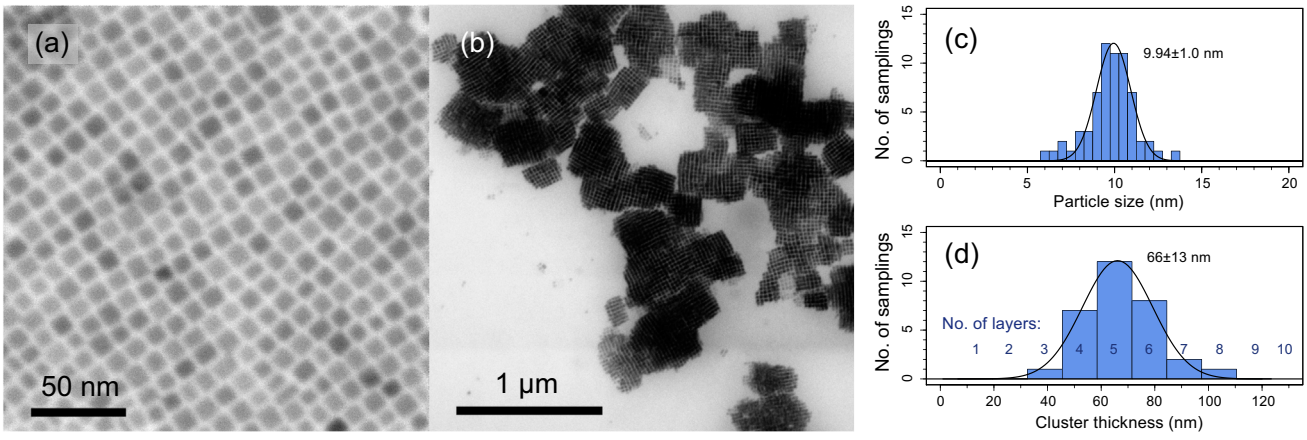

Fig. 1. Scanning transmission (STEM) images of (a) a monolayer of $CsPbBr_3$ QDs and (b) their 3D clusters; Statistical distributions of (c) edge-length and (d) cluster thickness of QDs, also expressed in numbers of QD layers considering an interparticle gap of 3 nm.

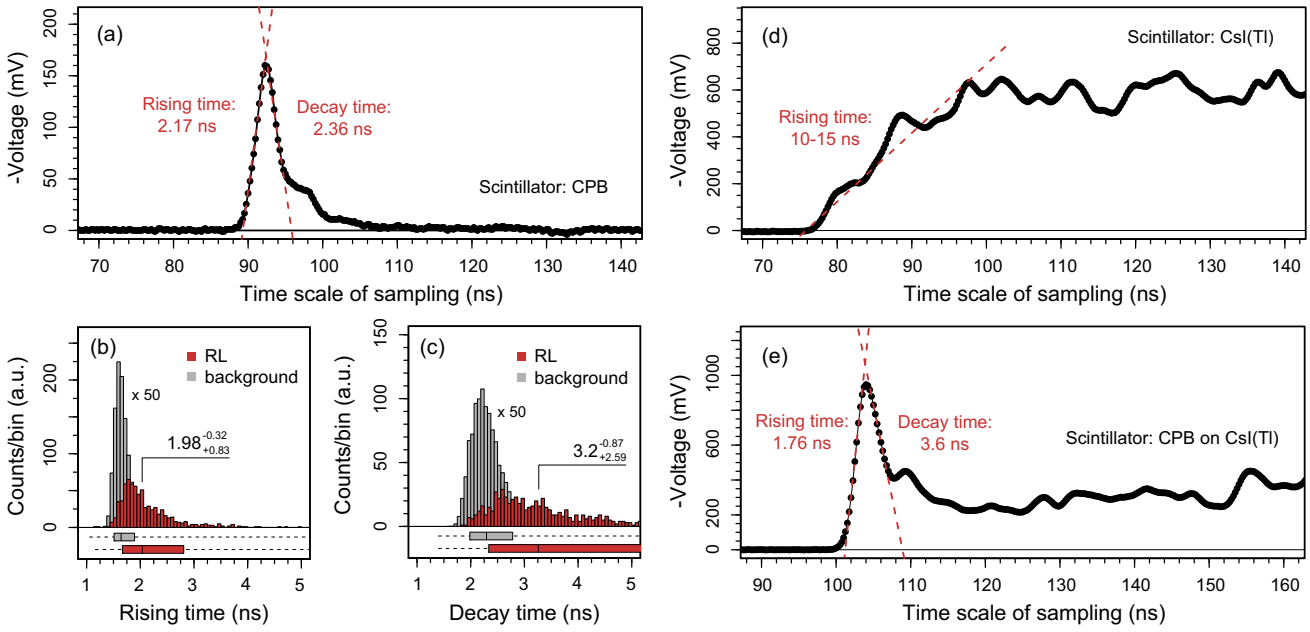

Fig. 2. (a) Pulse waveform of a typical signal recorded with the 4 GS/s pulse digitizer for an α-particle-induced radioluminescent flash from $CsPbBr_3$ nanoclusters; (b, c) Distributions of rising times and decay times defined by 10–90% voltage transition for non-selected (grey) and coincidence-selected (red) signals; (d, e) Pulse waveforms from a 3-mm thick conventional CsI(Tl) scintillator without and with a deposited layer of $CsPbBr_3$ nanoclusters, respectively.

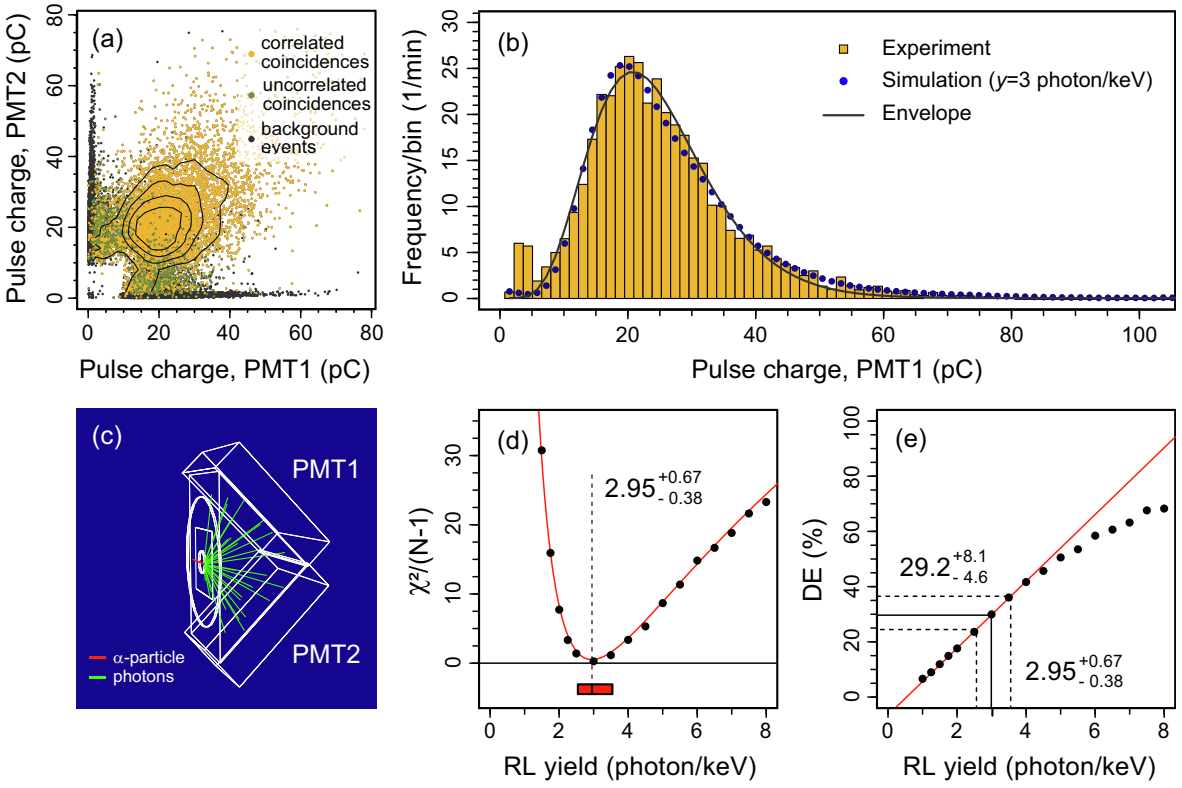

Fig. 3. (a) Correlation plot of pulse charges measured by the PMTs. Contour lines mark the frequency of real coincidence events after subtracting the contributions of uncorrelated pulses; (b) Comparison of experimental and simulated pulse-charge distributions assuming y = 3 photon/keV; (c) Schematic view of simulation geometry showing a typical RL flash; (d) Goodness of fit in terms of Pearson's χ^2-test. The range of best-fit RL yield (red bar) was obtained for φ = 0.1–0.2; (e) Detection efficiency (DE) for clusters of 5 QD-layers determined by the simulated proportionality with RL yield.

every photoelectron generated at the PMT cathode gives a measurable pulse smeared by the electron-gain variance. The DE was found 29.2% at the best-fit RL yield, which was regarded as a theoretical (zero-threshold) estimate representing an upper bound for practical situations due to the unavoidable loss of subthreshold pulses.

4. Conclusion

In conclusion, the utilization of luminescent $CsPbBr_3$ perovskite QDs is anticipated as nanoscaled scintillators for charged-particle detection when extreme timing precision is required. In comparison with conventional particle-detection techniques, perovskite nanomaterial-based devices certainly exhibit short transition times concerning other semiconductors [23,24], thus remarkably improving the efficiency of high data-flow measurements. The RL yield and DE were estimated for QD clusters, which propose systematic studies on radiation-sensing properties of perovskite nanomaterials.

Declaration of Competing Interest

The authors declare that they have no known competing financial interests or personal relationships that could have appeared to influence the work reported in this paper.

Acknowledgments

This work is supported by GINOP-2.3.2-15-2016-00041 and GINOP-2.3.3-15-2016-00029 projects co-financed by the European Union and the European Regional Development Fund. Instrumentation was partly provided by the project VKSZ_14-1-2015-0021 of Széchenyi 2020 Program. L. Csige is grateful for the support of the Bolyai János Research Scholarship of the Hungarian Academy of Sciences.

Appendix A. Supplementary data

Supplementary data to this article can be found online at https://doi.org/10.1016/j.matlet.2021.129398.

References

[1] F. Hu, H. Zhang, C. Sun, et al., ACS Nano 9 (2015) 12410–12416.
[2] L. Chouhan, S. Ghimire, Ch. Subrahmanyam, et al., Chem. Soc. Rev. 49 (2020) 2869–2885.
[3] Z. Song, J. Zhao, Q. Liu, Inorg. Chem. Front. 6 (2019) 2969–3011.
[4] Y.-F. Li, J. Feng, H.-B. Sun, Nanoscale 11 (2019) 19119–19139.
[5] C.R. Kalaiselvi, N. Muthukumarasamy, D. Velauthapillai, et al., Mater. Lett. 219 (2018) 198–200.
[6] Z. Shi, A. Jayatissa, Materials 11 (2018) 729.
[7] J. Yuan, A. Hazarika, Q. Zhao, et al., Joule 4 (2020) 1160–1185.
[8] G. Náfrádi, E. Horváth, M. Kollár, et al., Energy Convers. Manage. 205 (2020) 112423.
[9] L. Protesescu, S. Yakunin, M. Bodnarchuk, et al., Nano Lett. 15 (2015) 3692–3696.
[10] Q. Akkerman, G. Rainó, M. Kovalenk, et al., Nat. Mater. 17 (2018) 394–405.
[11] M.A. Becker, R. Vaxenburg, G. Nedelcu, et al., Nature 553 (2018) 189–193.
[12] S. Yakunin et al., Nat. Photon. 9 (2015) 444–449.
[13] Q. Chen, J. Wu, X. Ou, et al., Nature 561 (2018) 88–93.
[14] Y. Zhang, R. Sun, X. Ou, et al., ACS Nano 13 (2019) 2520–2525.
[15] L. Shen, Y. Fang, D. Wang, et al., Adv. Mater. 28 (2016) 10794–10800.
[16] H. Wei, J. Huang, Nat. Commun. 10 (2019) 1066.
[17] Y. He, Z. Ltriu, K.E.A. McCall, Nucl. Instrum. Methods A 922 (2019) 217–221.
[18] E. Graham, D. Gooding, J. Gruszko, et al., J. Instrum. 14 (2019) P11024.
[19] V.K. Ravi et al., Nanotechnology 27 (2016) 325708.
[20] K. Nordlund, J. Nucl. Mater. 520 (2019) 273–295.
[21] E. de Jong, G. Yamashita, L. Gomez, et al., J. Phys. Chem. C 121 (2017) 1941–1947.
[22] M. Rafipoor, R. Koll, J. Merkl, et al., Small 15 (2019) 1803798.
[23] B. Lv, H. Zhang, L. Wang, et al., Nat. Commun. 9 (2018) 1536.
[24] D. Aldakov, P. Reiss, J. Phys. Chem. C 123 (2019) 12527–12541.

Charged-particle induced radioluminescence in nanoclusters of $CsPbBr_3$ perovskite quantum dots

Mátyás Hunyadi, Csaba Buga, Lóránt Csige, Attila Csík

Institute for Nuclear Research (ATOMKI), Debrecen H-4026, Hungary

Email: hunyadi.matyas@atomki.hu

Supplementary Data

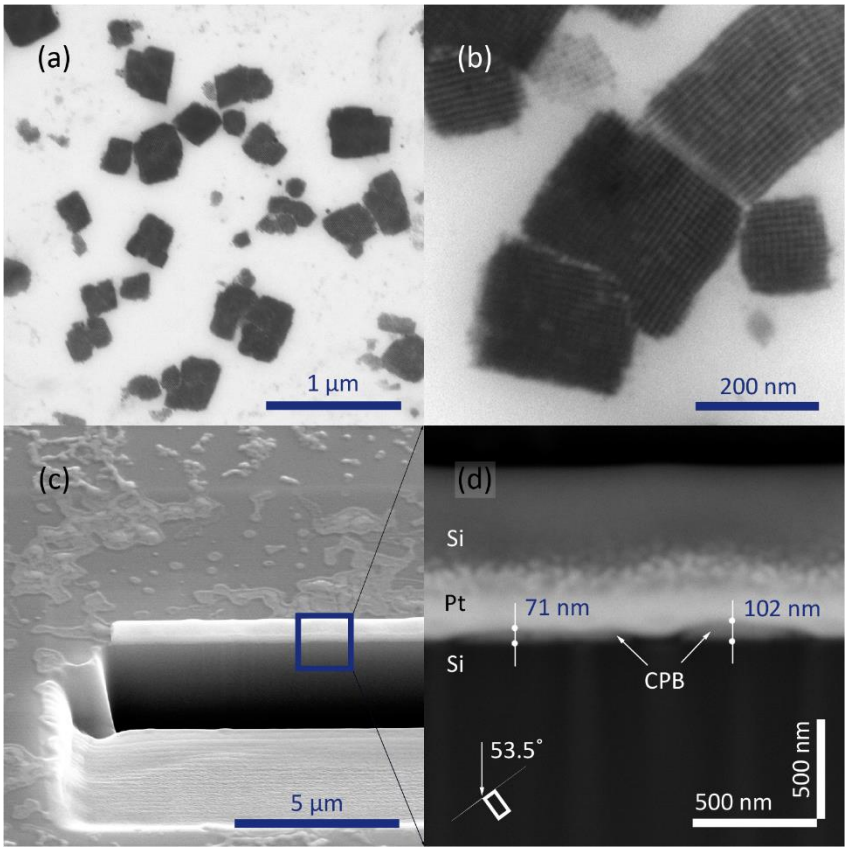

Figure S1: (a,b) Scanning TEM (STEM) images of the $CsPbBr_3$ (CPB) nanoclusters at different magnifications deposited on a Cu-grid; (c) tilted-angle SEM image of CPB clusters deposited on a Si substrate at the location of cross-cutting well prepared with Ga^+-beam etching; (d) zoomed part marked on panel c showing the cross-section view of the CPB clusters buried under a protecting Pt layer. The distribution of cluster thickness was determined by the statistical evaluation of cross-section images.

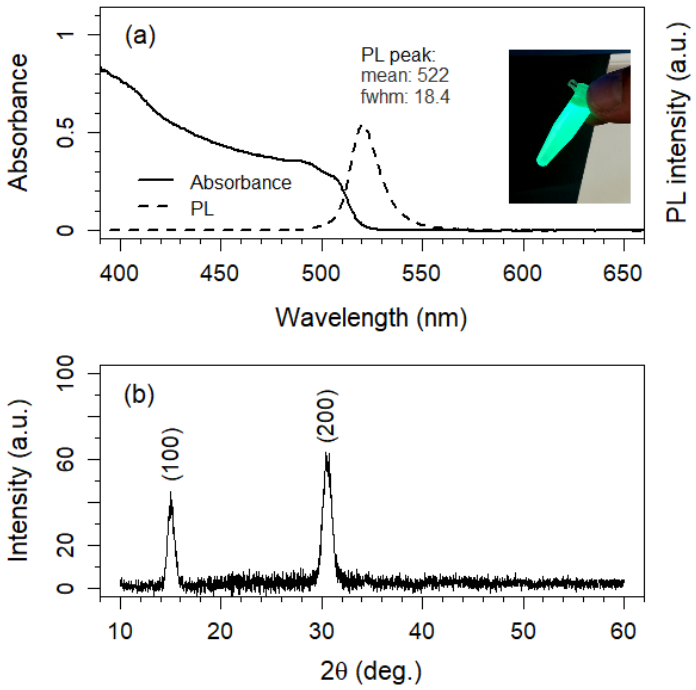

Figure S2: (a) Absorption and emission spectra of $CsPbBr_3$ QDs. The inset shows the luminescence of QD suspension in 365-nm UV light. (b) XRD pattern of $CsPbBr_3$ QDs deposited on the glass substrate.

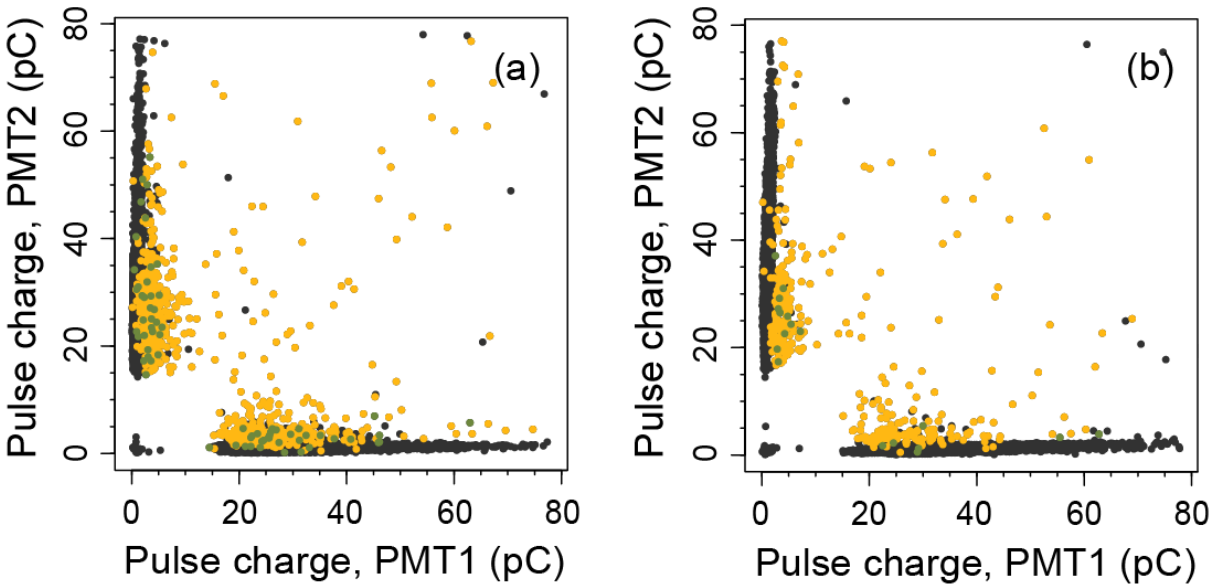

Figure S3: Pulse-charge correlation plots of control measurements with bare glass substrate replacing the CPB layer (a) with and (b) without the α-source. Black and colored dots represent uncorrelated (singles) and correlated (coincidence) luminescence events, respectively.